Axial shape asymmetry and high-spin states in nuclei with $Z = 100$ suggested by the projected total energy surface approach

Tu Ya (图雅),[1] Yong-Jing Chen (陈永静) ⦿,[2,*] Yong-Shou Chen (陈永寿),[3,†] Zao-Chun Gao (高早春),[3,4] and Ling Liu (刘玲)[1]

[1]*School of Physics Science and Technology, Shenyang Normal University, ShenYang 110034, China*
[2]*China Nuclear Data Center, China Institute of Atomic Energy, Beijing 102413, China*
[3]*China Institute of Atomic Energy, Beijing 102413, China*
[4]*State Key Laboratory of Theoretical Physics, Institute of Theoretical Physics, Chinese Academy of Sciences, Beijing 100190, China*

The axial-shape asymmetry of yrast states in $^{246-256}$Fm is studied by performing the projected total-energy surface (PTES) calculations, which consider the beyond-mean-field effects associated with the restoration of rotational symmetry and shape variation at the same time. The results show a large elongation deformation but also a considerable large triaxiality for their ground and high spin states, the triaxial deformation $\gamma \approx 11°$ in average. In comparison, the TRS calculations have also been performed for these nuclei, and the results show a well-established axial quadrupole shape in their ground states. The presence of the significant triaxial deformation can be attributed to the beyond-mean-field effects generated by the angular-momentum projection. The axial asymmetric shape for the yrast states of nuclei with $Z = 100$, suggested by the present variation after projection (VAP) calculations, indicates that the triaxial degree of freedom may also play a significant role in other transfermium and even superheavy nuclei. The present PTES calculations have well reproduced the available experimental energies of the ground-band states and predict the rest yrast states up to spin 30 in each nucleus. The calculated yrast bands of $^{246-256}$Fm present the back bending phenomenon at about the state 18^+, caused by the alignment excitations of the two quasiparticle neutrons of $\nu j_{15/2}[743]7/2$ or of $\nu h_{11/2}[761]1/2$. It is worth confirming the predicted band structures by the future spectroscopic experiments in the transfermium nuclei for the study of the single-particle structure in the superheavy mass region.

I. INTRODUCTION

One of the important predictions in nuclear physics is the emergence of a region of long-lived superheavy elements (SHE) beyond the actinides, the so-called "island of stability." Exploring the island is the current goal in nuclear science. In the past few years, researchers have made significant progress in the synthesis of new elements [1,2], and, just recently, the new elements 113, 115, 117, and 118 have been named. It is instructive to realize that the existence of SHE is attributed to the nuclear shell effect because the macroscopic liquid drop model would predict nonexistence of such heavy elements due to large Coulomb repulsion. Consequently, the location of the island depends sensitively on single-particle structures in the highest mass region. Therefore, in parallel to the synthesis experiments, spectroscopy study is also very important. Because the synthetic cross section of the superheavy nucleus is extremely small, the experimental spectroscopic study of superheavy nuclei encounters a great challenge.

Recently, a big progress in γ-ray spectroscopy has been obtained, that is the measurements of low-lying states of the transfermium nuclei. By studying the single-particle structures of the transfermium nuclei one may gain useful information on the relevant single-particle states of SHE [3–5]. Both the in-beam spectroscopy and spectroscopy following the decay of isomeric states or α decays have been used to study nuclei with $Z \approx 100$ and $N \approx 150$–160 [6–10]. The transfermium nuclei are the gateway to the SHE region, and they are strongly deformed, the extracted experimental quadrupole deformation parameter is $\beta = 0.25$–0.30. At such large deformations, the down-slopping single particle orbitals originating from spherical subshells, which play an important role in the SHE region, can come down close to the Fermi surface in the transfermium nuclei. This gives us a great chance to study the structures of superheavy nuclei through the investigation of low-lying states of transfermium nuclei. The spectroscopy experiments also suggest that the exotic nonaxial-octupole deformation (potato shape), may exist in transfermium nuclei as the negative-parity bands with the bandhead of 2^-, which were well reproduced by the reflection asymmetric shell model with the Y_{32} deformation component [11], and this was further supported by multidimensional constraint covariant density-functional theory [12]. The presence of nonaxial-octupole deformation implies the large priority to have the nonaxial-quadruple deformation. Of course, the more strong experimental signature of the triaxiality may be the presence of the low-lying γ bands observed in the transfermium region.

*ahchenyj@126.com
†yschen@ciae.ac.cn

Several theoretical approaches have been used to study transfermium nuclear structure, such as the nuclear shapes, the properties of rotational states and the shell structures. Nuclear shapes are essential for determining various observables, such as moments of inertia, transitional quadrupole moments, and transition properties. In most of the analysis, the mean-field model and cranked shell model (CSM) have been employed. Although these models have been shown to provide a reasonable description of the structures of transfermium nuclei, it is known that they do not conserve a good angular momentum. The nuclear rotation is not fully described in quantum mechanics, but described semiclassically by introducing the rotational frequency, instead of angular momentum, in the CSM. The projected shell model (PSM) and the reflection asymmetry shell model (RASM) can restore the broken rotational symmetry through the angular-momentum-projection, and, therefore, describe the rotational states in good quantum number of angular momentum. The HFB, as the typical mean-field theory, has been widely used and successfully describes the bulk properties of nuclei in almost the entire mass region. However, the more accurate descriptions of the ground and low-lying states require the inclusion of the beyond mean-field effects by carrying out the projections of quantum numbers onto the eigenstates. Our recent calculations of the HFB vacuum states for the even-even sd-shell nuclei by performing the simultaneous projections of the angular momentum I, isospin T, and mass number A onto the eigenstates, demonstrated that the impact of the angular-momentum projection, the I states, is most important on both the energy and the shape change, and, in contrast, the TA states still have a large discrepancy in energy and results in no shape change relative to the HFB states, see Ref. [13] for details. For the present study the contribution of the particle number projection is negligible, but this effect may be considered for the study that is sensitive to the particle number conservation, for example, of the transfer reaction. The current PSM and RASM calculations, however, have been performed with a fixed deformation, which is not determined self-consistently but by fitting the data. The interplay between nuclear shapes and rotational motion has long been an interesting topic in nuclear physics. The potential-energy surface (PES) calculations have been frequently used in this research direction. The PES approach allows the shape variation and provides a self-consistent way to determine the deformation through the energy minimization procedure. One of PES approaches has been the total Routhian surface (TRS), which is based on the CSM, and thus provides the energy surface at a given rotational frequency, not an angular momentum. To consider the beyond-mean-field effects associated with the rotational symmetry restoration, the projected total-energy surface (PTES) theory has been formulated based on the triaxial projected shell model (TPSM) [11,14] hybridized with the macroscopic-microscopic (MM) model [15,16]. The PTES describes the total-energy surface of a deformed nucleus with the good angular-momentum quantum number. The total energy of an atomic nucleus is decomposed into the macroscopic, microscopic, and rotational terms.

In the PTES, the macroscopic and microscopic parts are described with the liquid drop model and the Strutinsky method of shell effects, respectively, and the rotational energy

is given by the TPSM, as the beyond-mean-field term. The basic framework of the PTES is similar to the TRS [17], but the key difference between the two approaches is the fact that the PTES has the energy surface carrying good angular momentum and the TRS provides the energy surface having a rotational frequency, not quantum number. The advantage of the PTES approach is manifested by the fact that the energy surfaces correspond to each of the given spins so that the minima determine the nuclear states with the good quantum number of angular momentum, and theoretical results can then be compared directly with the experimental data in the laboratory frame. This theory has been recently used to investigate the impact of the beyond-mean-field effects on the triaxiality in the light tungsten system, and it has been demonstrated to provide an accurate description of the observed properties [15,16]. In the present study, we have extended the PTES calculation of the rare-earth nuclei to the transfermium mass region for the description of the yrast band states of nuclei with $Z = 100$, with an emphasis on the triaxiality of the yrast states, and on the band structure which is associated with the quasiparticle (q.p.) excitations. A similar construction of the total energy in the laboratory frame has been successfully applied to the energy curve calculation, energy as function of elongation deformation, in the studies of the collectivity of neutron-rich nuclei [18] and the shape-coexisting rotation of neutron-deficient nuclei [19]. We note that two similar calculations were previously down for the transfermium nuclei with the PSM and TPSM theories, respectively, and valuable results were obtained. The PSM calculation in Ref. [3] investigates the alignments of the high-j orbits in the rotational bands of the transfermium nuclei, which considers sufficient shell-model configurations up to four quasiparticles, but the γ deformation was not considered. The TPSM method employed in Ref. [14] includes only the vacuum configuration, no q.p. configurations, and, therefore, no shell-model configuration mixing was considered, and we note that the method is valid for the description of the γ vibrational states. In the present TPES as well as TPSM calculations, we have, however, included both the γ deformation and the shell-model configuration mixing of the quasiparticle configurations up to four quasiparticles. The inclusion of the q.p. configurations is crucial for the studies of very high spin states beyond the band crossing.

A brief description of the model is presented in Sec. II. The results of calculations and discussions are given in Sec. III. Conclusions are in Sec. IV.

II. THE PROJECTED TOTAL-ENERGY SURFACE THEORY

The projected total energy of the nuclear system, as a function of deformations ε_2, γ, and ε_4, for a given spin I may be given as

$$E_{\text{tot}}^I(N, Z, \beta) = E_{MM}(N, Z, \beta) + E_{\text{rot}}^I(N, Z, \beta), \quad (1)$$

where β represents a set of deformation parameters $(\varepsilon_2, \gamma, \varepsilon_4)$. $E_{MM}(N, Z, \beta)$ is the total energy of the nucleus at rest, which can be calculated by the MM model, including the macroscopic liquid-drop model energy [20], the microscopic shell correction and the pairing correction energy in

the standard Strutinsky method [21,22]. For simplicity and more clear structure of the theory the pairing correction is not considered in the present calculation, and it was checked that inclusion of pairing correction does not change the results of minima, although the energy surface becomes a bit complex in the region apart from the minimum. The term of $E_{\mathrm{rot}}^{I}(N, Z, \beta)$ is the rotational energy obtained by the TPSM, which can be further decomposed into the collective rotational term and the quasiparticle excitation induced by rotation [16]. The basic construction of the total energy is similar to that of the total Routhian in the total Routhian surface (TRS) method where the rotational energy is calculated microscopically as a function of the rotational frequency, namely, the difference between the expectation values of the Hamiltonian at the rotational frequency nonzero and zero by using the cranking wave function, $\langle \Psi^{\omega}|H|\Psi^{\omega}\rangle - \langle \Psi^{\omega=0}|H|\Psi^{\omega=0}\rangle$, see, for example, Refs. [17,23–25]. In addition, the q.p. excitation energy is calculated as the sum energy of the excited quasiparticles in the rotating frame at the frequency ω which belong to the given configuration.

The PTES described with Eq. (1) carries then the good quantum number of angular momentum through the rotational term, and the minimization procedure has to be performed for each given spin. Therefore, the PTES approach may be classified as the variation-after-projection (VAP).

The Hamiltonian of the TPSM is expressed as follows:

$$H = H_0 - \frac{1}{2}\sum_{\lambda=2}^{4}\chi_\lambda \sum_{\mu=-\lambda}^{\lambda}Q_{\lambda\mu}^{\dagger}Q_{\lambda\mu} - G_0 P_{00}^{\dagger}P_{00}$$

$$-G_2 \sum_{\mu=-2}^{2}P_{2\mu}^{\dagger}P_{2\mu}, \qquad (2)$$

where H_0 is the spherical single-particle Hamiltonian, which contains a proper spin-orbit force [26]. The second term is the quadrupole-quadrupole (QQ) interaction that includes the nn, pp, and np components. In normal spectroscopic calculation of TPSM, the interaction strength is determined in a self-consistent way with the quadrupole deformation, refer to Ref. [27]. In the energy-surface calculation, the QQ interaction strength χ should be, however, fixed during the calculation, namely, keep a constant for each deformation mesh point. The problem for the adoption of the interaction strength arises then due to hundreds of deformation points. But, unfortunately, the strength has not yet been given in a commonly known way. We suggest a rule that this quadrupole interaction strength may be obtained in the self-consistent way from the TPSM theory with respect to a proper one of the deformation mesh points. In the present calculation, the values of the strength χ are determined in a self-consistent way with the equilibrium deformation corresponding to the local minimum of the Strutinsky's energy surface of $E_{LD} + E_{\mathrm{shell}}$. Consequently, our PTES calculation has to include two steps, namely, first Strutinsky's energy surface to obtain the interaction strength and finally the PTES. Note that two kinds of energy surface are not required to have exactly same mesh structure, and this allows us to reduce the computation time. The third term in the Hamiltonian is the monopole pairing,

whose strength parameter G_0 (in MeV) is determined by the expression $G_0 = (g_1 \mp g_2 \frac{N-Z}{A})A^{-1}$, where the minus (plus) sign stands for neutrons (protons) and $g_1 = 21.02$ and $g_2 = 13.23$ are fixed for all the nuclei studied in this article. The last term is the quadrupole pairing, whose strength parameter G_2 may be calculated from $G_2 = f G_0$, usually $f = 0$–0.2, we set $f = 0.13$, which is found to be appropriate for this mass region [28]. In the present calculation, the hexadecapole deformation is not considered as a variable and taken as of $\varepsilon_4 = 0$.

The TPSM wave function is expressed by means of the projection operator,

$$|\Psi_{IM}\rangle = \sum_{K\kappa} F_{\kappa,K}^{I}\hat{P}_{MK}^{I}|\Phi_\kappa\rangle, \qquad (3)$$

in which the projected multiquasiparticle states span the shell-model space. In Eq. (3), $|\Phi_\kappa\rangle$ represents the set of multiquasiparticle states labeled by κ, and for the considered even-even Fm nuclei it includes up to the 4 q.p. states associated with the triaxially deformed q.p. vacuum $|0\rangle$, $\alpha_{\nu_1}^{\dagger}\alpha_{\nu_2}^{\dagger}|0\rangle$, $\alpha_{\pi_1}^{\dagger}\alpha_{\pi_2}^{\dagger}|0\rangle$, and $\alpha_{\nu_1}^{\dagger}\alpha_{\nu_2}^{\dagger}\alpha_{\pi_1}^{\dagger}\alpha_{\pi_2}^{\dagger}|0\rangle$. The triaxially deformed single-particle states are generated by the Nilsson Hamiltonian. In the present TPSM calculation, three major shells of $N = 5, 6, 7$ for neutrons and $N = 4, 5, 6$ for protons are considered, and the pairing correlations are included by a subsequent BCS calculation for the Nilsson states. $\hat{P}_{MK}^{I}$ in Eq. (3) is the three-dimensional angular-momentum-projection operator [27]. The rotational energies together with the wave functions, i.e., the coefficients $F_{\kappa,K}^{I}$, are obtained by solving the eigenvalue equation,

$$\sum_{K\kappa}F_{\kappa K}^{I}\left(\langle\Phi_{\kappa'}|H P_{K'K}^{I}|\Phi_\kappa\rangle - E^{I}\langle\Phi_{\kappa'}|P_{K'K}^{I}|\Phi_\kappa\rangle\right) = 0. \qquad (4)$$

In the present approach, $E_{MM}(N, Z, \beta)$ in Eq. (1), provides the energy of the deformed BCS vacuum state, relative to the spherical liquid drop energy, and the rotational energy $E_{\mathrm{rot}}^{I}(N, Z, \beta)$ is calculated by Eq. (4), relative to the deformed q.p. vacuum. The total energy of the deformed nuclear system, E_{tot}^{I} in Eq. (1), is consequently defined in the laboratory frame, which is a function of spin and also has a good parity. The nuclear equilibrium deformation for each of the yrast or low-excited states can be obtained by minimizing their respective total energy with respect to the deformation parameters ε_2 and γ. Once the PTES is calculated the minimization procedure can be performed straight by finding the local minimum in the total-energy surface at each spin, and by this way the equilibrium deformations for a given spin are determined self-consistently.

III. RESULTS AND DISCUSSION

A. Projected total-energy surface for given angular momentum

All calculations of the projected total-energy surfaces in the present work are carried out for a given angular momenta as well as a given parity; this allows us to obtain the nuclear states with good quantum numbers of spin and parity and, therefore, provides an opportunity to make a direct comparison between the theory and the experiment. The general features of the projected total-energy surfaces for the ground
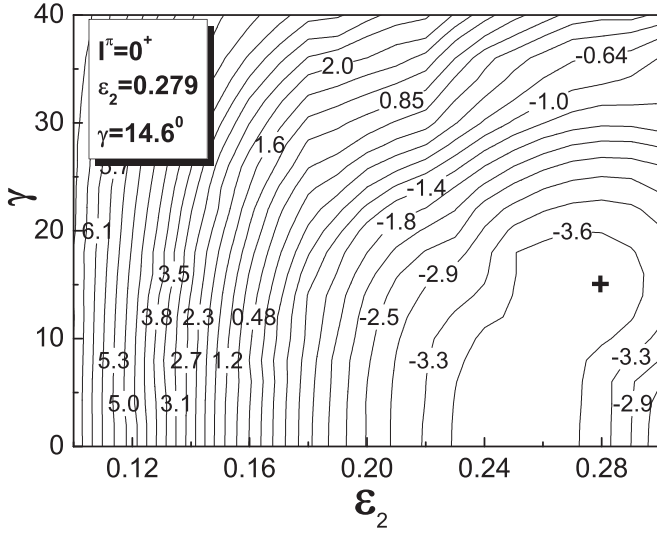
FIG. 1. Contour plot of total energy in units of MeV for the ground state of ^{248}Fm, the local minimum is marked by "+." The γ axis is given in units of degrees.

state (g.s.) $I^{\pi} = 0^{+}$ are illustrated with the example of the ^{248}Fm in Fig. 1. In the present PTES calculations, the range of the elongation deformation ε_2 is taken from 0.1 to 0.3, while the range of the triaxial deformation γ from $0°$ to $40°$, and the mesh points of 20 have been taken for both the ε_2 and γ deformations. Figure 1 shows that there exists a local minimum in the PTES for the g.s. of ^{248}Fm, which represents the equilibrium deformations of $(\varepsilon_2 = 0.279, \gamma = 14.6°)$. The results imply that the g.s. of the nucleus is well-deformed, and it is particularly noteworthy to have a considerable axial asymmetry with $\gamma \approx 15°$.

B. Projected total-energy surface for the yrast states in the $^{246-256}$Fm isotopes

The PTES calculation for ^{248}Fm in the g.s. $I^{\pi} = 0^{+}$, demonstrated in the above section, has been extended to the yrast states of the $^{246-256}$Fm isotopes, up to spin 30. A local minimum is found in each of the 96 PTESs for spins

of $I^{\pi} = 0^{+}, 2^{+}, 4^{+}, 6^{+}, \ldots, 30^{+}$ in the yrast bands of these six nuclei. These local minima allow us to determine the equilibrium deformations (ε_2, γ) for each spin in the yrast states of the $^{246-256}$Fm isotopes, and the results are listed in Table I. Both the elongation and triaxial equilibrium deformations being almost unchanged with increasing spin for each of the selected Fm isotopes, characterizing well-deformed rotor, with the exception of ^{254}Fm and ^{256}Fm where some change of ε_2 deformation has been found after spin 18^{+}, for example, increasing from 0.24 to 0.28 in ^{254}Fm and from 0.25 to 0.28 in ^{256}Fm. The deformation change in the two nuclei reflects the deformation-driving effects induced by the two q.p. alignment excitation of the high-j orbital, a detail discussed below. The very small absolute values of γ obtained from the TRS calculations indicate the axial symmetry for the g.s. of $^{246-256}$Fm isotopes, while the considerably large γ deformations obtained from the PTES calculations implies the axial asymmetry nature of the g.s. for these nuclei. Note that the present PTES and TRS calculations start with the same single-particle states and approximately same pairing interaction as well as the same model space truncation, and the major difference is the fact that the former contains the angular-momentum projection but the latter does not. Therefore, we may safely conclude that the beyond-mean-field effect, associated with the angular-momentum projection, may be the origin of the triaxiality of $^{246-256}$Fm obtained from the PTES calculation.

It is shown in Table I the ε_2 deformation of the ground states in $^{246-256}$Fm presents some decreasing with increasing neutron number, for example, the ε_2 values are about 0.28 for ^{246,248}Fm and about 0.24 for ^{250,252,254,256}Fm. The decreasing-in-ε_2 deformation with increasing neutron number may be understood as shell effects. Specifically, the neutron shell effects associated with the pronounced energy gap at neutron number 150, as shown in Fig. 2, may be responsible for the decrease of the ε_2 deformation in the Fm isotopes with mass number equal to and larger than 250. The triaxial deformation of $\gamma \approx 14°$ is found for ^{246,248}Fm and a smaller value of $\gamma \approx 10°$ for ^{250,252,254,256}Fm, as shown in Table I. The slight γ deformation change may be explained as the neutron shell effects again. In the neutron single-particle Nilsson diagram,

TABLE I. Deformations of the yrast states of $^{246-256}$Fm isotopes determined by the energy minima in PTES for spins 0^{+} to 30^{+}.

|	I^{π}	0^{+}	2^{+}	4^{+}	6^{+}	8^{+}	10^{+}	12^{+}	14^{+}	16^{+}	18^{+}	20^{+}	22^{+}	24^{+}	26^{+}	28^{+}	30^{+}
^{246}Fm	ε_2	0.276	0.276	0.277	0.277	0.277	0.277	0.278	0.284	0.284	0.284	0.284	0.284	0.284	0.284	0.278	0.277
	γ	13.4°	13.4°	13.4°	13.4°	13.4°	13.4°	13.4°	13.2°	13.2°	13.2°	13.2°	13.2°	13.2°	13.2°	13.4°	13.4°
^{248}Fm	ε_2	0.279	0.279	0.279	0.279	0.279	0.279	0.279	0.279	0.279	0.279	0.279	0.279	0.279	0.279	0.279	0.279
	γ	14.6°	14.6°	14.6°	14.6°	14.6°	14.6°	14.6°	14.6°	14.6°	14.6°	14.6°	14.6°	14.6°	14.6°	14.6°	14.6°
^{250}Fm	ε_2	0.248	0.248	0.248	0.248	0.248	0.248	0.248	0.248	0.248	0.248	0.248	0.248	0.248	0.246	0.246	0.250
	γ	8°	8°	8°	7°	7°	7°	6.8°	6.4°	6.2°	5.8°	5.6°	5.2°	5.0°	4.2°	4.0°	5.0°
^{252}Fm	ε_2	0.242	0.242	0.242	0.242	0.242	0.243	0.243	0.243	0.244	0.244	0.244	0.231	0.231	0.231	0.231	0.232
	γ	10°	10°	10°	10°	10°	10°	10°	9.8°	9.8°	9.6°	9.6°	10.6°	10.6°	10.6°	10.6°	11.4°
^{254}Fm	ε_2	0.242	0.242	0.242	0.242	0.244	0.244	0.244	0.244	0.244	0.282	0.282	0.282	0.282	0.282	0.282	0.282
	γ	10.2°	10.2°	10.2°	10.2°	10.4°	10.2°	10.2°	10°	9.8°	7°	7°	7°	7°	7°	7°	7°
^{256}Fm	ε_2	0.246	0.246	0.246	0.246	0.246	0.246	0.246	0.248	0.248	0.280	0.280	0.280	0.282	0.282	0.270	0.270
	γ	11.4°	11.4°	11.4°	11.4°	11.4°	11.2°	11.2°	11.2°	11.2°	9.8°	9.4°	9.4°	9.4°	9.4°	9°	9°
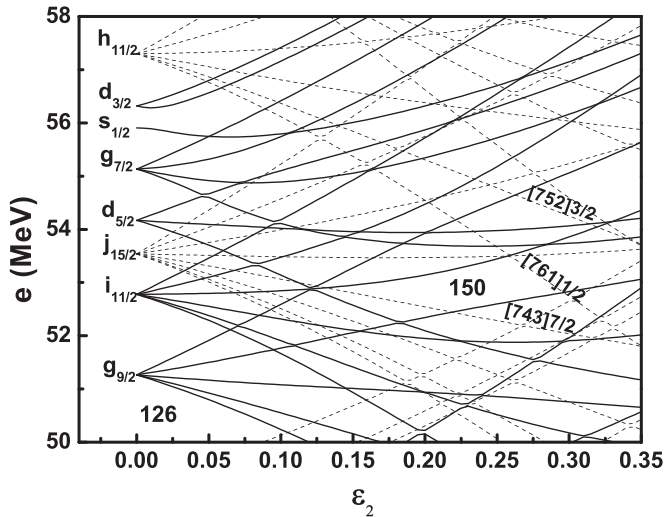
FIG. 2. Neutron Nilsson diagram showing single-particle orbitals as deformation ε_2 varies. Orbitals with positive (negative) parity are shown by solid (dashed) curves.

the single-particle energy as a function of γ at $\varepsilon_2 = 0.27$, there exist an energy gap of $N = 148$ and persists in a large range of the triaxial deformation, from $\gamma = 10°$ to $30°$. The associated shell effects may be responsible for the γ deformation of ^{246,248}Fm being about four degrees larger than the heavier Fm isotopes. We note that the employed neutron single-particle diagram created by using the Nilsson parameter of Bengtsson and Ragnarsson [26] is very similar to the diagram calculated with the Wood-Saxon potential [29].

The PTES for each state of spin and parity is first calculated, and then the minimization procedure with respect to the elongation and triaxial deformations is performed to obtain the energy of the state together with the equilibrium deformations. In this way, the yrast band is calculated self-consistently within the PTES approach, and it is the variation after projection (VAP) calculation. Figure 3 shows the calculated yrast bands for the $^{246-256}$Fm isotopes, the corresponding equilibrium deformations are given in Table I, compared with the experimental data [6,30,31]. It is seen that the calculated results are in very good agreement with the experimental data.

The calculated yrast bands of $^{246-256}$Fm present the back bending phenomenon at about the state 18^+, caused by the alignment excitation of two q.p. neutrons. One can extract the moment of inertia and find the corresponding band-crossing frequency from the calculated yrast band energies $E(I)$, just as it has been shown from experimental band energies in many publications. The calculated moment of inertia in function of the rotational frequency, $J_1(\omega)$ shows the upper bending at the band-crossing frequencies of $\hbar\omega_c = 0.32$, 0.28, 0.26, and 0.29 MeV in ^{246}Fm, ^{248}Fm, ^{250}Fm, and ^{252}Fm, respectively, as shown in Fig. 4. These upper bendings are caused by the angular-momentum alignments of two q.p. neutrons of $\nu j_{15/2}[743]7/2$, according to the analysis of the components in the calculated wave functions. The calculated moments of inertia present a strong back bending at the band-crossing frequency of $\hbar\omega_c = 0.30$ MeV for both ^{254}Fm and ^{256}Fm, as shown in Fig. 4, where the back bending is caused by the alignments of two q.p. neutrons of $\nu h_{11/2}[761]1/2$, which is a strong down-slopping high-j orbital in the Nilsson diagram, as shown in Fig. 2, and, thus, it may generate the driving force that leads to an increase of the elongation deformation in these
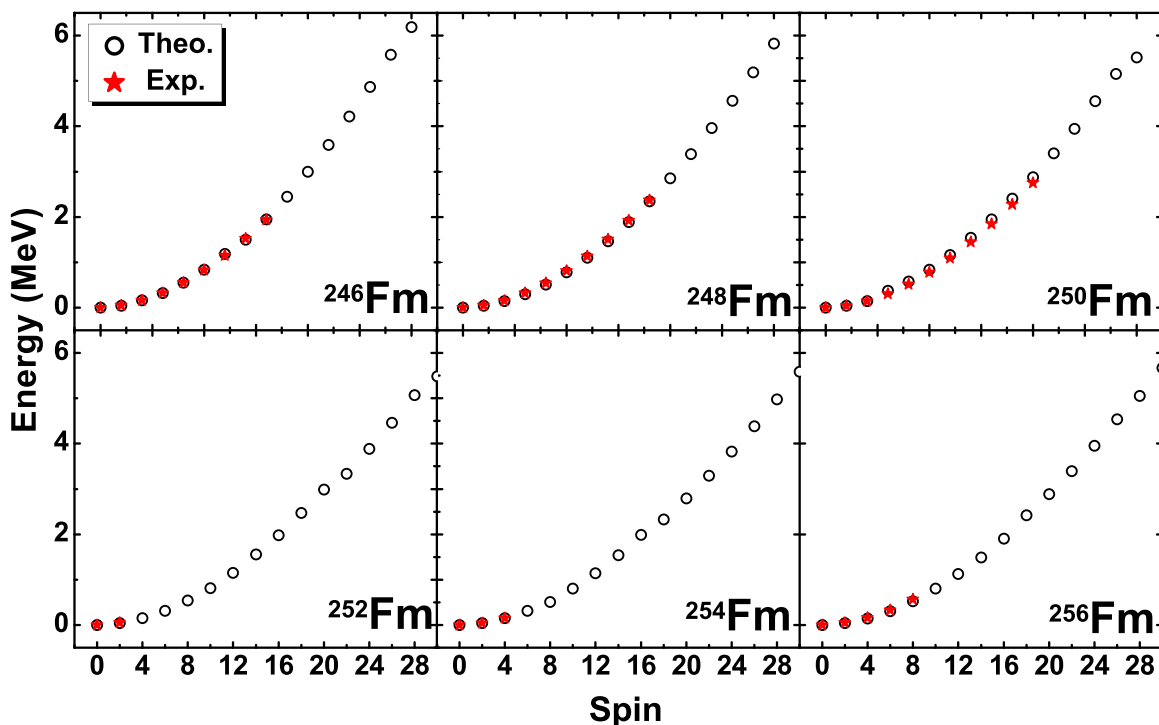

FIG. 3. Calculated yrast bands, the energy levels, for $^{246-256}$Fm isotopes compared with the experimental data.
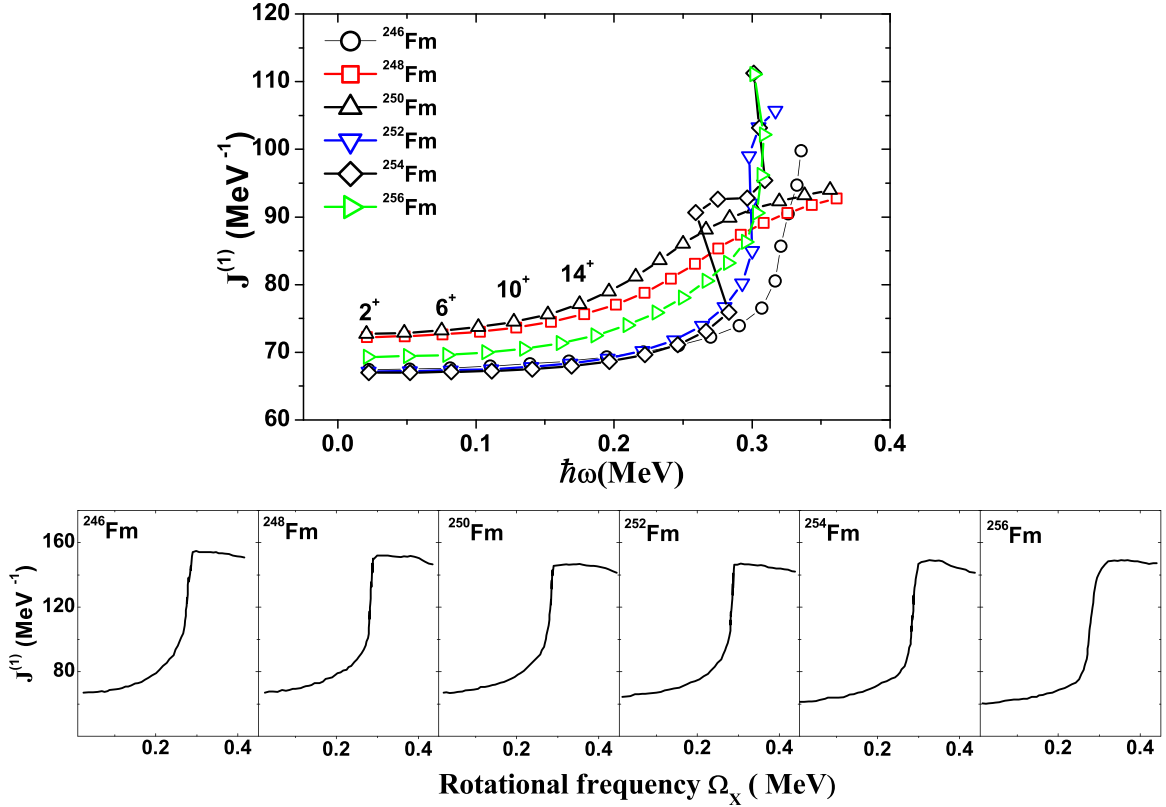
FIG. 4. Moment of inertia as function of rotational frequency for $^{246-256}$Fm. The upper panel shows the results of the present calculations, each symbol point corresponds to an initial state of the $E2$ transition, whose I^π value is marked above symbols for few points only as guide. As a comparison, the bottom panel shows the results of the CRHB calculations, and the data are measured by reading the part of Fm isotopes of Fig. 12 in Ref. [32].

two nuclei, as discussed above, in addition to being responsible for the back bending. As a check, the upper bending and back bending together with values of the corresponding crossing frequencies have been confirmed by the TPSM calculations with the quadrupole deformations of the ground states determined by the PTES calculations. The situation is similar to the back bending phenomenon that occurs in rare-earth even-even nuclei, where the pair of two q.p. neutrons of $i_{13/2}$ breaks and align their angular momenta along the rotational axis. The critical spin at which the two q.p. band crosses the ground state band is about $12\hbar$ experimentally in rare-earth nuclei, while it has been predicted in the present calculation to be about $18\hbar$ in transfermium nuclei. Recently, the covariant density-functional theory predicts the back bending phenomenon in the transfermium nuclei, and the cranked relativistic Hartree-Bogoliubov (CRHB) calculations in Ref. [32] report the band crossing frequencies of $\hbar\omega = 0.25$, 0.26, 0.28, 0.27, 0.26, and 0.25 MeV for ^{246}Fm, ^{248}Fm, ^{250}Fm, ^{252}Fm, ^{254}Fm, and ^{256}Fm, respectively, as shown in the bottom panel of Fig. 4. It is seen that both the present PTES calculations and the CRHB calculations, which are of typically different methods, predict the presence of the back bending phenomenon in $^{246-256}$Fm, with not too much difference in band-crossing frequencies. In Ref. [3], the rotational alignment of high-j orbitals and the back-crossing phenomenon in the yrast bands of Cf, Fm, and No isotopes were carefully discussed by analyzing the experimental data and the calculated yrast states

with PSM theory. The major difference between the PSM calculation and the present work is the fact that the latter includes the γ degree of freedom, and the deformations are determined self-consistently for each spin to gain the prediction power of the theory.

We note that the nature of the back bending phenomenon in $^{246-256}$Fm implies the detailed structure of the single-particle states, in particular, the level scheme of the high-j orbits across the major shell. The present calculations reveal that the predicted band crossing arises from the alignment of neutron orbital $\nu h_{11/2}[761]1/2$ which locates right at the neutron shell gap of $N = 184$, a highly attentive new magic number. The predicted location of this high-j orbital implies its importance for the understanding of nuclear structures for the superheavy nuclei. And, therefore, the experimental yrast spectroscopy of $^{246-256}$Fm becomes very worthy for probing the single-particle structures in the transfermium and superheavy mass regions.

C. Comparison between projected total-energy surface and total Routhian surface calculations

The total Routhian surface (TRS) approach has been extensively used to describe the shape of heavy nuclei, which is one of typical nuclear model based on the mean-field approximation but without including of the beyond-mean-field effects. It is, therefore, instructive to make a comparison between the
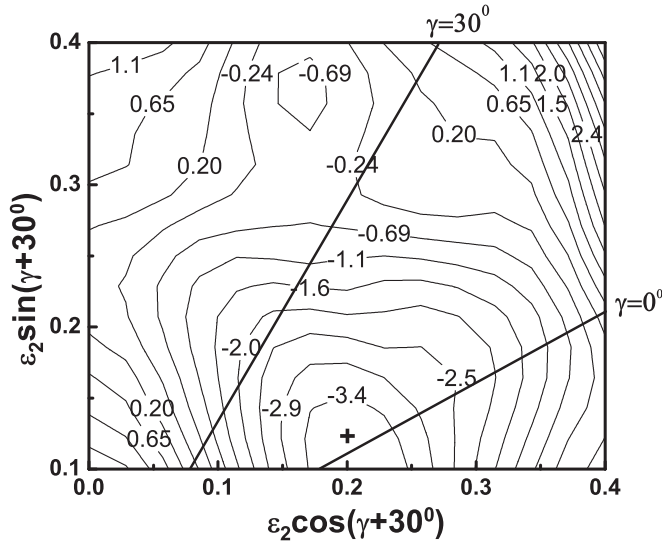
FIG. 5. Contour plot of total Routhian in units of MeV for ^{248}Fm, calculated at the rotational frequency $\hbar\omega = 0.02\hbar\omega_0$, the minimum is marked by "+."

PTES and TRS calculations. The rotational frequency, as a classical term employed in the TRS approach, has been a useful quantity to describe nuclear rotation. However, because of the semiclassical nature of the TRS method it is not possible to strictly describe even the ground state (g.s.), which has a good angular momentum of $I = 0$. It should be noticed that the quantum state with spin of $I = 0$ is a rotational one which does not match with the rotational frequency of zero. Usually, to describe the shape of the ground state of the nucleus, the TRS calculation may be, empirically, performed at a small rotational frequency which is larger than zero and far below the band-crossing frequency. As an example, the TRS for ^{248}Fm calculated at the rotational frequency of $\hbar\omega = 0.02\hbar\omega_0$ is shown in Fig. 5, which reports a local minimum at the deformations of ($\varepsilon_2 = 0.234$, $\gamma = 2°$). Table II shows the deformations of the ground states of $^{246-256}$Fm isotopes determined by the energy minima in TRS at the rotational frequency of $\hbar\omega = 0.02\hbar\omega_0$. The calculated elongation equilibrium deformations given by the TRS for all the considered nuclei are a bit smaller than those determined by the PTES method. The trend of changing of the resulting equilibrium elongation deformation, the slightly decreasing with increasing neutron number, is similar between the TRS and PTES calculations.

TABLE II. Deformations of the g.s. of $^{246-256}$Fm isotopes determined by the energy minima in the TRS at the rotational frequency of $\hbar\omega = 0.02\hbar\omega_0$.

	Nuclei					
	^{246}Fm	^{248}Fm	^{250}Fm	^{252}Fm	^{254}Fm	^{256}Fm
ε_2	0.234	0.234	0.224	0.224	0.224	0.224
γ	2°	2°	−3°	−3°	−3°	−3°

Recently, the global calculation across the nuclear chart of axial symmetry breaking was carried out by using the macroscopic-microscopic finite-range liquid-drop model (FRLDM) [33,34]. Many nuclear ground states have been predicted to be triaxially shaped or γ soft by the FRLDM calculations, some of which were previously predicted to be axially symmetric by the TRS calculations. The different results of the FRLDM with respect to the TRS method come from their different parametrizations, although the two methods belong to the same type of macroscopic-microscopic approach. For the $^{246-256}$Fm isotopes, both the FRLDM and TRS calculations report a axial symmetry for the ground states and the similar elongation deformation.

D. Triaxiality and γ bands

The triaxiality is found for $^{246-256}$Fm isotopes, the average value of the equilibrium triaxial deformation is $\gamma \approx 11°$. The origin of the triaxiality is attributed to the beyond-mean-field effects as having addressed above. In Fig. 6, we have made a comparison between the unprojected energy curve and the projected energy curves for the states with angular momentum $I^\pi = 0^+, 2^+, \ldots, 10^+$ in ^{248}Fm. In the left part of Fig. 6 showing the energies in function of ε_2 at a fixed value of $\gamma = 0$, the minimum at $\varepsilon_2 = 0.255$ is found in the projected energy curves, and the unprojected energy curve presents a similar form and minimum. The right part of Fig. 6 shows the energies as a function of γ at a fixed value of $\varepsilon_2 = 0.255$. It is seen that the unprojected energy curve has a well-defined minimum at about $\gamma = 3°$ and, however, the projected energy curves exhibit the very γ softness and a shallow minimum at about $\gamma = 18°$. This feature of the projected energy curves suggests that the inclusion of the projected energy could lead to the possible triaxial shape for the system which is predicted to have an axial symmetric shape within the mean-field approximation. Furthermore, the observed low-lying γ bands in the ^{254}Fm and ^{256}Fm may be regarded as the indirect evidence for the existence of the triaxiality in these nuclei. In the TPSM calculations for the γ bands, the elongation deformations have been taken as the same as the equilibrium elongation deformations for the ground states $I^\pi = 0^+$ (see Table I), while the values of the γ deformation have been taken to reproduce the excitation energies of the γ bands, adopted deformation values are $\gamma = 25.5°$ for ^{254}Fm and $\gamma = 24°$ for ^{256}Fm, respectively. The present TPSM calculations well reproduce the known experimental γ band data as well as the ground-state bands, as shown in Fig. 7. The energy of the γ-bandhead is sensitive to the γ deformation. The small change of the γ deformation, about few degrees, is crucial to reproduce the experimental data. Unfortunately, there are no more experimental data available for γ bands in these transfermium isotopes, and the systematic study of the γ bands in the $^{246-256}$Fm isotopes requires further experimental verifications. The presence of the γ bands in nuclei has been widely argued as the γ vibration around the prolate shape. It has been a long-standing puzzle that, in quite many deformed nuclei which are predicted by the mean-field models to have the axial symmetry and no γ softness, yet the low-lying γ bands have been observed experimentally. The TPSM, as a shell model
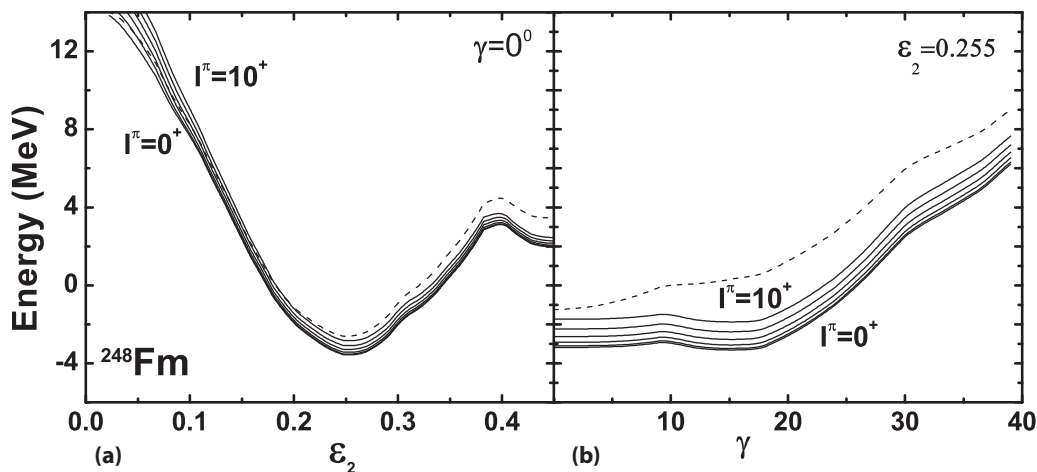
FIG. 6. Energy surfaces for states with angular momentum $I^\pi = 0^+, 2^+, \ldots, 10^+$. The energies are calculated as function of (a) quadrupole deformation ε_2 with $\gamma = 0°$, and (b) γ deformation with $\varepsilon_2 = 0.255$. Full (dashed) curves correspond to projected (unprojected) calculations. The γ axis is given in units of degrees.

by using the deformed basis, can describe the γ-vibrational bands in heavy deformed nuclei, with the rotational behavior similar to that of ground bands. The γ-vibrational states can be, as is common knowledge, interpreted as a mainly harmonic fluctuation about an axially symmetric shape. The present PTES calculations generally predict a considerable triaxiality and the pronounced gamma softness, as the results of the impacts of projecting unto a good angular momentum, in the ground states of heavy deformed nuclei. These results seem to offer somewhat useful information for understanding the wide occurrence of such low-lying γ-vibrational states whose excitation energies are about 0.6-0.8 MeV above the ground state, in rotational heavy nuclei.

The PTES-TPSM approach treats the nuclear rotation quantum mechanically and allows three-dimensional rotation through the angular-momentum projection. In contrast, the TRS-CSM method (not tilted cranking) treats the rotation of

quantum states in a semiclassical way by introducing rotational frequency and requiring the system to rotate around a fixed principle axis. Although the method has been very successful in the study of highly rotating nuclei, in particular with the selective efficiency in systematic analysis of the data, its disadvantage is, however, clear that it cannot properly account for the effects of the three-dimensional quantum rotation. The beyond-mean-field effect incorporated in the PTES-TPSM approach is the quantal effect that favors the triaxial rotation. Recently, the first study of the full projected mean field was performed for the even-even sd-nuclei by using the USDB Hamiltonian. The calculated results show that the intrinsic shapes of the VAP (variation after projection) wave functions with angular-momentum projection are always triaxial while the usual HFB methods provide axial shapes [13]. In our earlier work, our VAP energy calculations clearly show that the angular-momentum projection is very important to achieve
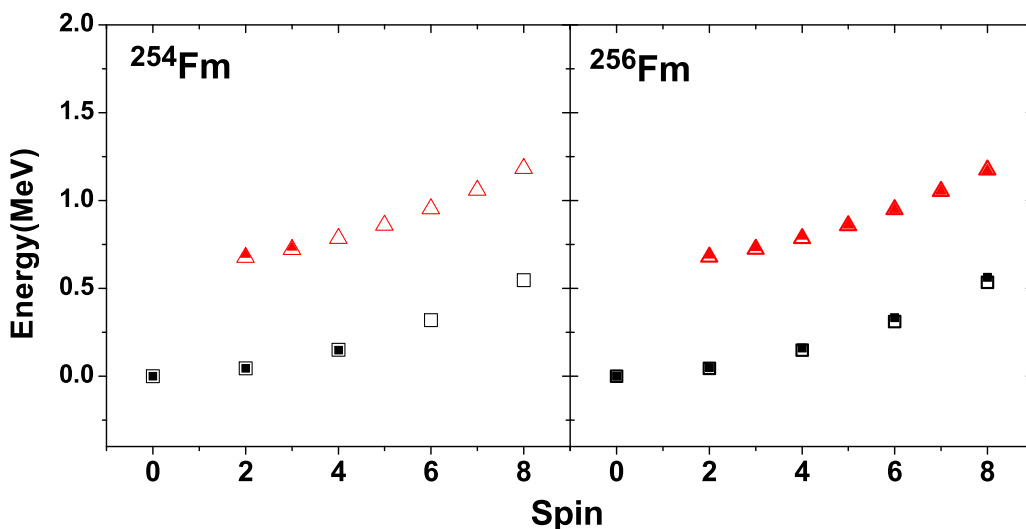

FIG. 7. Calculated g.s. bands (open squares) and their γ bands (open triangles), the energy versus spin for ^{254}Fm and ^{256}Fm and a comparison with the experimental data (solid symbols).
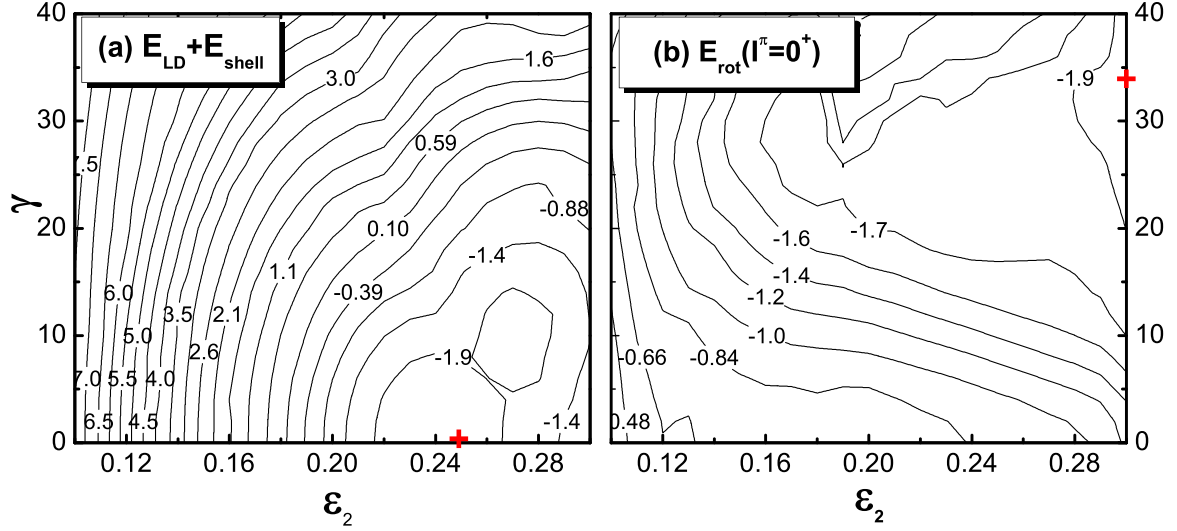
FIG. 8. Component energy surfaces of the total energy for the ground state of $I^\pi = 0^+$ in ^{248}Fm: (a) $E_{LD} + E_{shell}$ and (b) E_{rot}. The energy is in units of MeV. The γ axis is given in units of degrees.

a good approximation to the full shell model [35]. In addition, early other calculations of triaxial deformation and its effect on the low-energy nuclear structure phenomena performed by Bender *et al.* [36,37] using beyond-mean-field calculations based on the nonrelativistic Skyrme energy density functionals, by Rodríguez *et al.* [38,39] and Delaroche *et al.* [40] using beyond-mean-field calculations based on the Gogny DIS interaction, and by Yao *et al.* [41], by Nikšić *et al.* [42,43] using relativistic energy density functionals, come to a similar conclusion that beyond-mean-field effects play an important role in nuclear triaxiality. This conclusion was also supported by the Skyrme-HFB-QRPA calculation, which incorporates the fluctuation about the HFB-mean field, where the energies of the γ-vibration band states calculated for ^{24}Mg are in a good agreement with the experimental data [44].

E. Decomposition of energy surface

To study the beyond-mean-field effect associated with the angular-momentum projection in further detail, the component energy surfaces have been calculated as a decomposition of the PTES. The calculated component energy surfaces for ^{248}Fm are shown in Fig. 8(a) for $E_{LD} + E_{shell}$ and 8(b) for E_{rot}. The liquid drop model-plus-shell energy surface presents a local minimum at the axial symmetry with the $\varepsilon_2 \approx 0.25$, and the flatness of the surface around the minimum indicates a modest γ softness towards the γ-deformation direction. The rotational energy surface for the spin $I = 0$, shown in Fig. 8(b), presents the striking feature to drive the ε_2 deformation towards a larger elongation and the γ deformation from both $0°$ (prolate) and $60°$ (oblate) axial symmetric shapes towards a large triaxiality of about $35°$. It is seen that the projected rotational energy at $\varepsilon_2 = 0.25$ can generate a significant enough driving force in the γ direction to provide a lowering of the total energy in the laboratory frame by about 900 keV from the axial symmetry to the triaxiality of $\gamma \approx 15°$.

The $E_{LD} + E_{shell}$ surface shown in Fig. 8(a) applies also to the present TRS calculation so that the TRS shown in Fig. 5

can be regarded as the result by adding the rotational energy given by CSM to the liquid-drop-plus-shell energy. The axial symmetric shape described by the local minimum in the $E_{LD} + E_{shell}$ surface remains unchange in the TRS, implying that the γ-deformation driving effect promised from adding the classical rotational energy defined in the TRS approach is not sufficient to cause the formation of a local triaxial minimum in the TRS. In contrast, the quantal rotational energy surface such as one shown in Fig. 8(b) can provide the strong γ-deformation driving in the formation of the axial asymmetry shapes of the yrast states in ^{248}Fm.

Although a direct comparison between the quantal and classical rotational energies is not possible, it can be seen that, at $\varepsilon_2 = 0.25$, the energy lowering from $\gamma = 0°$ towards $15°$ is about 0.2 MeV for the classical rotation in the TRS at $\hbar\omega = 0.02\hbar\omega_0$, estimated by reading data from Fig. 5 and Fig. 8(a), and, however, it is about 0.9 MeV for the quantum rotation in the PTES at $I^\pi = 0^+$, estimated from Fig. 8(b). These results indicate that, in the nuclear energy surface calculations, the inclusion of the angular-momentum projection, as the beyond-mean-field effects, is crucial in the study of nuclear symmetry and symmetry break. We would like to emphasize that the quantal nuclear state at an angular momentum $I = 0$ is a certain rotational state which has the same essential nature as the one at $I > 0$, and the rotational energy surfaces at $I = 0$ and $I > 0$ will have a similar structure. However, the cranking nuclear state at the frequency $\hbar\omega = 0$ is not a rotational state, and the nuclear rotation is described at the frequency $\hbar\omega > 0$ in the CSM picture. Consequently, there is the fatal problem in the CSM to describe strictly the nuclear ground state that has a quantum number of $I = 0$.

IV. CONCLUSIONS

The axial asymmetry shape in even-even nuclei $^{246-256}$Fm has been studied by the projected total-energy surface (PTES) approach. The projected total-energy surfaces for the yrast states of $^{246-256}$Fm present the local triaxial

minima corresponding to the elongation equilibrium deformation of $\varepsilon_2 \approx 0.25$ and the triaxial deformation of $\gamma \approx 11°$. In contrast, the TRS calculations, as the typical mean-field approximation, yield the axial symmetric equilibrium shapes with the quadrupole deformations of ($\varepsilon_2 \approx 0.23$, $\gamma \approx 0°$) for the g.s. of the same nuclei. The experimental data of the yrast states of $^{246-256}$Fm have been very well reproduced by the present PTES calculation. By using the equilibrium elongation deformation determined by the PTES calculation and the γ deformation of $\approx 25°$, the TPSM calculations also well reproduce the available experimental excited γ bands of ^{254,256}Fm. The beyond-mean-field effects incorporated in the PTES approach through the angular-momentum projection are responsible for the presence of the significant triaxiality for the nuclei with $Z = 100$, which are previously predicted as axial symmetry within the mean-field approximation. According to the origin of the triaxiality together with the prediction power of the PTES full quantum-mechanical calculations one may expect that nuclei in the whole transfermium region and even in the superheavy nuclear region should be described by considering the γ degree of freedom.

The calculated yrast bands of $^{246-256}$Fm present the back bending phenomenon at about spin 18^+, caused by the alignment excitation of two q.p. neutrons of the high-j shell. According to the analysis of the wave functions, the upper bendings in ^{246,248,250,252}Fm may be attributed to the alignments of two q.p. neutrons of $\nu j_{15/2}[743]7/2$, while the strong back bendings in ^{254,256}Fm originate from the alignment excitation of two q.p. neutrons of $\nu h_{11/2}[761]1/2$. We note that the nature of the back bending phenomenon in $^{246-256}$Fm implies the specific structure of the single-particle states, in particular, the level scheme of the high-j orbits across the major shell. And, therefore, the experimental yrast spectroscopy of $^{246-256}$Fm is very worthy for probing the single-particle structure in the transfermium and superheavy-mass region.

ACKNOWLEDGMENTS

[1] S. Hofmann and G. Muenzenberg, Rev. Mod. Phys. **72**, 733 (2000).

[2] Y. Oganessian, Nucl. Phys. A **787**, 343 (2007).

[3] F. Al-Khudair, G. L. Long, and Y. Sun, Phys. Rev. C **79**, 034320 (2009).

[4] Y. Sun, Nucl. Phys. A **834**, 41 (2010).

[5] X. T. He, Z. Z. Ren and S. X. Liu, Nucl. Phys. A **817**, 45 (2009).

[6] J. E. Bastin *et al.*, Phys. Rev. C **73**, 024308 (2006).

[7] R. D. Herzberg *et al.*, Phys. Rev. C **65**, 014303 (2001).

[8] P. Reiter *et al.*, Phys. Rev. Lett. **82**, 509 (1999).

[9] R. D. Herzberg and P. T. Greenlees, Prog. Part. Nucl. Phys. **61**, 674 (2008).

[10] R. D. Herzberg and D. M. Cox, Radiochim. Acta **99**, 441 (2011).

[11] Y.-S. Chen, Y. Sun, and Z.-C. Gao, Phys. Rev. C **77**, 061305(R) (2008).

[12] J. Zhao, B. N. Lu, E. G. Zhao, and S. G. Zhou, Phys. Rev. C **86**, 057304 (2012).

[13] Z.-C. Gao, M. Horoi, and Y. S Chen. Phys. Rev. C **92**, 064310 (2015).

[14] Y. Sun, G.-L. Long, F. Al-Khudair, and J. A. Sheikh, Phys. Rev. C **77**, 044307 (2008).

[15] T. Ya, Y. S. Chen, Z. C. Gao, L. Liu, and Y. J. Chen, Phys. Rev. C **95**, 064316 (2017).

[16] T. Ya, Y. S. Chen, Z. C. Gao, S. Y. Yu, and L. Liu, Sci. China: Phys., Mech. Astron. **57**, 2054 (2014).

[17] T. Ya, Y. S. Chen, S. Y. Yu, C. W. Shen, Z. C. Gao, Y. J. Chen, and L. Liu, Nucl. Phys. A **848**, 260 (2010).

[18] C. F. Jiao, J. C. Pei, and F. R. Xu, Phys. Rev. C **90**, 054314 (2014).

[19] C. F. Jiao, Yue Shi, H. L. Liu, F. R. Xu, and P. M. Walker, Phys. Rev. C **91**, 034309 (2015).

[20] W. D. Myers and W. J. Świątecki, Ark. Fys. **36**, 343 (1967).

[21] V. M. Strutinsky, Nucl. Phys. A **95**, 420 (1967).

[22] V. M. Strutinsky, Nucl. Phys. A **122**, 1 (1968).

[23] W. Nazarewicz, J. Dudek, R. Bengtsson, T. Bengtsson, and I. Ragnarsson, Nucl. Phys. A **435**, 397 (1985).

[24] W. Satula, R. Wyss, and P. Magierski, Nucl. Phys. A **578**, 45 (1994).

[25] F. R. Xu, W. Satula, and R. Wyss, Nucl. Phys. A **669**, 119 (2000).

[26] T. Bengtsson and I. Ragnarsson, Nucl. Phys. A **436**, 14 (1985).

[27] Z. C. Gao, Y. S. Chen, and Y. Sun, Phys. Lett. B **634**, 195 (2006).

[28] R. D. Herzberg *et al.*, Nature (London) **442**, 896 (2006).

[29] R. R. Chasman, I. Ahmad, A. M. Friedman, and J. R. Erskine, Rev. Mod. Phys. **49**, 833 (1977).

[30] J. Piot, B. J.-P. Gall, O. Dorvaux, P. T. Greenlees, N. Rowley, L. L. Andersson, D. M. Cox, F. Dechery, T. Grahn, K. Hauschild, G. Henning, A. Herzan, R. D. Herzberg, F. P. Hessberger, U. Jakobsson, P. Jones, R. Julin, S. Juutinen, S. Ketelhut, T. L. Khoo *et al.*, Phys. Rev. C **85**, 041301(R) (2012).

[31] H. L. Hall, K. E. Gregorich, R. A. Henderson *et al.*, Phys. Rev. C **39**, 1866 (1989).

[32] A. V. Afanasjev and O. Abdurazakov, Phys. Rev. C **88**, 014320 (2013).

[33] P. Möller, R. Bengtsson, B. G. Carlsson, P. Olivius, and T. Ichikawa, Phys. Rev. Lett. **97**, 162502 (2006).

[34] P. Möller, A. J. Sierk, R. Bengtsson, H. Sagawa, and T. Ichikawa, At. Data Nucl. Data Tables **98**, 149 (2012).

[35] T. Ya, Yan He, Z.-C. Gao, J.-Q. Wang, and Y. S. Chen, Phys. Rev. C **95**, 064307 (2017).

[36] M. Bender and P. H. Heenen, Phys. Rev. C **78**, 024309 (2008).

[37] B. Bally, B. Avez, M. Bender, and P. H. Heenen, Phys. Rev. Lett. **113**, 162501 (2014).

[38] T. R. Rodríguez and J. L. Egido, Phys. Rev. C **81**, 064323 (2010).

[39] T. R. Rodríguez, Phys. Rev. C **90**, 034306 (2014).

[40] J. P. Delaroche, M. Girod, J. Libert, H. Goutte, S. Hilaire, S. Peru, N. Pillet, and G. F. Bertsch, Phys. Rev. C **81**, 014303 (2010).

[41] J. M. Yao, J. Meng, P. Ring, and D. Vretenar, Phys. Rev. C **81**, 044311 (2010).

[42] K. Nomura, N. Shimizu, D. Vretenar, T. Nikšić, and T. Otsuka, Phys. Rev. Lett. **108**, 132501 (2012).

[43] T. Nikšić, P. Marević, and D. Vretenar, Phys. Rev. C **89**, 044325 (2014).

[44] K. Yoshida and N. Van Giai, Phys. Rev. C **78**, 064316 (2008).